Article

NURBS-Based Collocation Methods for the Structural Analysis of Shells of Revolution

Maria Laura De Bellis [1,†] and Edoardo Artioli [2,*,†]

[1] Department of Innovation Engineering, Università del Salento, via per Monteroni, 73199 Lecce, Italy; marialaura.debellis@unisalento.it

[2] Department of Civil Engineering and Computer Science, University of Rome "Tor Vergata", via del Politecnico 1, 00133 Rome, Italy

[*] Correspondence: artioli@ing.uniroma2.it; Tel.: +39-06-7259-7014; Fax: +39-06-7259-7005

[†] These authors contributed equally to this work.

Abstract: In this work we present a collocation method for the structural analysis of shells of revolution based on Non-Uniform Rational B-Spline (NURBS) interpolation. The method is based on the strong formulation of the equilibrium equations according to Reissner-Mindlin theory, with Fourier series expansion of dependent variables, which makes the problem 1D. Several numerical tests validate convergence, accuracy, and robustness of the proposed methodology, and its feasibility as a tool for the analysis and design of complex shell structures.

1. Introduction

The application of differential quadrature or collocation methods for the solution of engineering boundary value problems dates back to the initial works by Bellmann and Casti [1,2], who are credited to have introduced the term differential quadrature operator, as the counterpart of quadrature operator for the approximation of a differential operator, *i.e.*, the strong form of the equation; and having applied this strategy to first-order ordinary non-linear differential equations. The terminology of collocation method is, to the best of the authors' knowledge, associated with the work by Petersen [3], and subsequently with the work by Karpilovskaya [4], Vainikko [5,6] and Kaspshitskaya [7]. The two methods share substantial similarities, namely the main idea of solving the strong form of the problem with a proper choice of discrete function spaces of approximation. By introducing a proper interpolation of the dependent variables, which is substituted in the governing differential equations, a linear set of equations for the unknown variables can be written by enforcing (*i.e.*, collocating) the discretized form of the governing equations at a set of locations on the domain, known as collocation points.

The method appears to have gained more interest in the scientific research community in the last two decades, rather than immediately following the presentation in the scientific literature. Nowadays, there is discussion as to whether this methodology may become a valid and general purpose alternative to more established methods such as the finite element method [8]. Without trying to give a general answer to this question, and without trying to provide a detailed literary review of the many applications of the collocation or differential quadrature method in past works, the aim of the present communication is to present an innovative formulation of the collocation method for the analysis of shells of revolution based on Non Uniform Rational B-Spline (NURBS) functions.

The collocation method is ideal in application to structural theories and has found several instances in the scientific literature [9]. With reference to the analysis of shell structural elements, Mirfakhraei and

Redekop [10] applied a Lagrangian differential quadrature method to the study of buckling phenomena of orthotropic thin shells of revolution; Wu *et al* [11,12] presented solutions to problems of axisymmetric bending of shells of revolution, introducing the so-called generalized differential quadrature rule. Viola and Artioli [13,14] and Artioli *et al.* [15,16] proposed a Lagrange differential quadrature solution for complex rotational shells with Fourier series expansion of dependent variables, both for the free vibration analysis, and for the static analysis of shells of revolution subject to unsymmetrical loading. The application of a collocation or differential quadrature method using Spline interpolants had been already proposed by Bellman and co-workers to solve general fourth-order differential equation problems [17], and later applied by Zhong and Guo [18,19] to static and buckling problems for Kirchhoff plates and to the non-linear free vibration analysis of straight Euler beams, respectively. Dade Huang proposed a Spline based collocation method for laminated plates and shells [20], while Viswanathan introduced the collocation method with Spline basis function in application to shear deformable laminated plates and shells [21–23].

The recent exponential growth of the isogeometric analysis [24–29] has raised attention on collocation methods based on NURBS and/or T-Splines trial functions. Given their higher-order smoothness and their favorable approximation properties, NURBS basis functions constitute an efficient interpolation tool for collocating differential operators, *i.e.*, for the approximation of the strong formulation of PDEs; furthermore they apply even to irregular or complex geometric domains. The newly developed IGA Collocation methods [8,30–33], set in the realm of weighted residuals [35], have been applied to a variety of solid, structural mechanics and engineering problems, with excellent performances in terms of efficiency, accuracy and robustness if compared to standard Galerkin methods.

The objectives of this work are the development and validation of the proposed methodology as an efficient, accurate numerical tool for the analysis and design of shells of revolution. The paper is organized as follows. In section 2 we formulate the differential problem of free vibration and of static equilibrium for a shell of revolution in the framework of Reissner-Mindlin theory. In this section, consistent cross-reference to Appendix A—Fundamental relationships for shells of revolution—and Appendix B—Equilibrium and boundary conditions operators—is made to make treatment more concise. In Section 3 some introductory elements on B-Splines are recalled from classic geometrical interpolation theory. Section 4 presents the basic one-dimensional NURBS interpolation basis functions as a result of certain projective transformations of B-Spline function spaces and its application to the NURBS-based collocation method, object of the present work. Section 5 collects an extensive set of numerical tests focused on the analysis of the convergence properties of the proposed method, as well as the validation in terms of accuracy and robustness by comparison with existing results. Last, the collocation method is applied to a problem of design for a complex shell structure, showing its feasibility as a numerical tool for engineering applications. Conclusions and future work perspectives are drawn in Section 6.

2. Statement of the Problem

2.1. Geometry

We consider a shell of revolution defined by its mid-surface, obtained by rotating a plane generator curve around an axis to form a closed surface, as shown in Figure 1a. Curvilinear coordinates on the mid-surface are chosen to be associated to two families of mutually orthogonal curvilinear lines over the mid-surface, *i.e.*, meridians and parallels, respectively. In particular, z is the coordinate measured along the axis of rotation, any value of z indicates a fixed parallel, whereas θ is the circumferential angle, indicating a given meridian. The third orthogonal coordinate is ζ, the distance of a point from

the mid-surface, measured along **n**, the outward unit normal to the mid-surface. The shell thickness will be denoted by t. Thus, the mid-surface can be described by the bounded open set:

$$\Omega = \{(z, \theta, \zeta) \in \mathbb{R}^3 | (z, \theta, \zeta) \in (z_i, z_f) \times [0, 2\pi] \times \{0\}\} \tag{1}$$

and its boundary

$$\partial\Omega = \{(z, \theta, \zeta) \in \mathbb{R}^3 | (z, \theta, \zeta) \in \{z_i, z_f\} \times [0, 2\pi] \times \{0\}\} \tag{2}$$
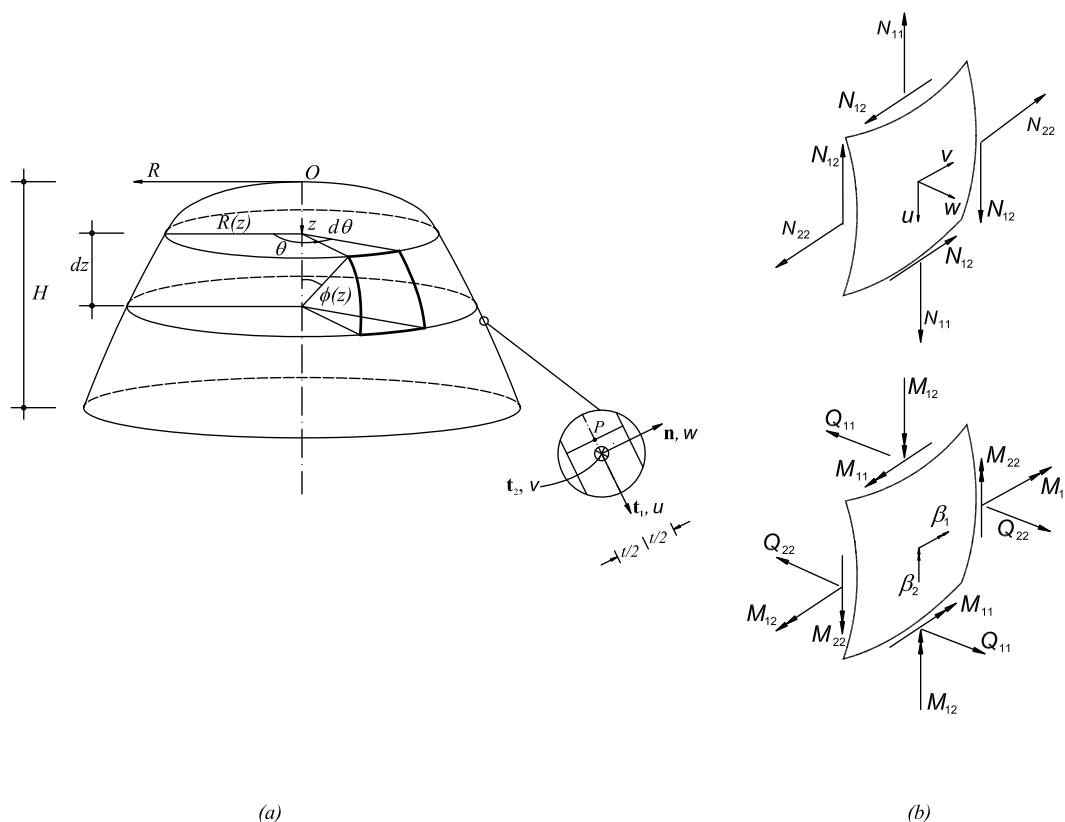

(a)　　　　　　　　　　　　　　　　　　　　　　　　　　　*(b)*

Figure 1. Geometry of shells of revolution.

For subsequent developments, it is here assumed that description of shell geometry is given in terms of the parallel radius equation $R = R(z)$, which defines the shape of the meridian curve, plus the thickness variation $t = t(z)$, for $z \in [z_i, z_f]$. Nonetheless, it is pointed out that this hypothesis is not mandatory: $R(z)$ and $t(z)$ need not be specified analytically; *i.e.*, they can be obtained from interpolated data, for instance with the use of NURBS basis functions [36]. According to the above geometry description, metrics of the shell of revolution mid-surface are resumed in Appendix A.

2.2. Displacement Field

Following the classical Reissner-Mindlin theory [37,38], and referring to Figure 1a, the displacements of a material point of the shell are u, v, and w, where u is the translation along $\mathbf{t}_1$, the unit vector tangent to the mid-surface and directed along the local meridian, v is the translation along $\mathbf{t}_2$, the unit vector tangent to the mid-surface and directed along the local parallel, and w is the displacement along $\mathbf{n}$, orthogonal to the mid-surface. Moreover, β_1 and β_2 represent the rotation of $\mathbf{n}$ about meridian $\mathbf{t}_1$ and circumferential $\mathbf{t}_2$ direction, respectively. In accordance with the aforementioned

theory, the components u and v vary linearly with respect to ζ, while w, β_1, and β_2 are constant through the thickness. The degrees of freedom are collected in the algebraic vector:

$$\mathbf{u}(z,\theta) = [u \ v \ w \ \beta_1 \ \beta_2]^\mathrm{T} \tag{3}$$

depending on the mid-surface coordinates z and θ.

2.3. Internal Actions

In the present theory, equilibrium equations are written in terms of internal actions, or stress resultants and couples per curvilinear coordinate line unit length, defined as the integrals of the stress components through the shell thickness [37]. In Figure 1b, stress resultants and couples are represented acting on a mid-surface element, identified by two couples of curvilinear coordinate lines, having in-plane outward normal unit vectors $\mathbf{t}_1$ and $\mathbf{t}_2$, respectively. These internal actions can be grouped as membrane normal N_{11}, N_{22}, [resp. shearing N_{12}] forces; flexural bending M_{11}, M_{22}, [resp. twisting M_{12}] couples; and transverse shear forces Q_{11}, and Q_{22}, respectively. The set of stress resultants and couples are collected in the algebraic vector:

$$\mathbf{S}(z,\theta) = [N_{11} \ N_{22} \ N_{12} \ M_{11} \ M_{22} \ M_{12} \ Q_{11} \ Q_{22}]^\mathrm{T} \tag{4}$$

Finally, $\mathbf{q}(z,\theta) = [q_u \ q_v \ q_w \ 0 \ 0]^\mathrm{T}$ are surface distributed load components per unit mid-surface area corresponding to the degrees of freedom $\mathbf{u}$. Surface distributed bending loads are not considered in the present development.

2.4. Equilibrium

Following classical arguments [38], the free vibration problem, as well as the static equilibrium problem for a shell of revolution, are formulated as a set of five differential equations for the internal actions, a format which is classified as statically indetermined [37]. Nevertheless, the above problem may be formulated as five differential equations for displacements and rotations plus boundary conditions, introducing proper shell-like strain measures, defined through a strain-displacement linear differential operator and choosing an isotropic linear elastic constitutive law between internal actions and strain components (see Appendix A). The strain components are conjugate to internal actions $\mathbf{S}$, and are collected in the algebraic vector:

$$\boldsymbol{\varepsilon}(z,\theta) = [\varepsilon_{11} \ \varepsilon_{22} \ \varepsilon_{12} \ \kappa_{11} \ \kappa_{22} \ \kappa_{12} \ \chi_1 \ \chi_2]^\mathrm{T} \tag{5}$$

where ε_{11}, ε_{22} [resp. ε_{12}] are membrane normal [resp. membrane shearing] strains, κ_{11}, κ_{22} [resp. κ_{12}] are bending normal [resp. bending twisting] curvature variations, while χ_{11}, and χ_{22} are transverse shearing strains. The equilibrium formulation amounts to a set of five linear differential equations for displacements and rotations $\mathbf{u}(z,\theta)$ on the two dimensional domain Ω, plus boundary conditions on $\partial\Omega$.

Applying Fourier series expansion of dependent variables (3), (4), and (5) with respect to the circumferential angle θ, the latter form can be reduced to a series of sets of five linear differential equations for the displacement harmonic amplitudes, on a one dimensional domain: the meridian curve. Since this treatment is quite consolidated [37–40], and the present work focuses on the Fourier series form of the equilibrium operator, for conciseness, we hereby present the displacement formulation in the so called harmonic form, postponing notations and the above recalled intermediate derivations to Appendices A and B.

2.4.1. Free Vibration Problem

The free vibration problem is governed by the classical linear eigenvalue problem:

$$
\begin{cases}
\text{Find } (\mathbf{u}^{(j)}, \omega^{(j)}) \text{ s.t. for any natural number } j, \\
\mathcal{L}^{(j)}(\mathbf{u}^{(j)}) = (\omega^{(j)})^2 \, \mathcal{M} \mathbf{u}^{(j)}, \ \forall z \in (z_i, z_f), \\
\mathcal{B}^{(j)}(\mathbf{u}^{(j)}) = \mathbf{0}, \ z \in \left\{ z_i, z_f \right\}
\end{cases}
\tag{6}
$$

where $(\mathbf{u}^{(j)}, \omega^{(j)})$ is the couple formed by the jth eigen-mode harmonic amplitude (in the sense specified in (35)), and the associated natural frequency. The inertia operator $\mathcal{M}$ is here taken as:

$$
\mathcal{M} = \rho A_1 R \, \text{diag} \left\{ t \ \ t \ \ t \ \ t^3/12 \ \ t^3/12 \right\}
$$

where ρ is the material mass density [38].

2.4.2. Static Equilibrium Problem

The static equilibrium problem is governed by the following linear elliptic problem:

$$
\begin{cases}
\text{Find } \mathbf{u}^{(j)} \text{ s.t. for any natural number } n, \\
\mathcal{L}^{(j)}(\mathbf{u}^{(j)}) = \mathbf{q}^{(j)}, \ \forall z \in (z_i, z_f), \\
\mathcal{B}^{(j)}(\mathbf{u}^{(j)}) = \mathbf{0}, \ z \in \left\{ z_i, z_f \right\}.
\end{cases}
\tag{7}
$$

The equilibrium operator $\mathcal{L}^{(j)}$ and the boundary conditions operator $\mathcal{B}^{(j)}$ appearing in (6) and (7) are reported in Appendix A, depending on the equation $R = R(z)$, *i.e.*, on the meridian shape, and on the relative metric quantities.

3. B-Spline Basis Functions

Non-Uniform Rational B-Splines - NURBS - are obtained from linear combination of B-Splines basis functions locally defined over patches of intervals [41]. A B-Spline of degree p is defined through an ordered set of non-decreasing coordinates in the parametric space: the knot vector $\Xi = \{\xi_1 = 0, \xi_2, \ldots, \xi_{n+p+1} = 1\}$, where p represents the polynomial degree of the interpolation, and n is the number of basis functions associated to the knot vector. Consequently, it results that $p = 0, 1, 2, 3 \ldots$ refers to constant, linear, quadratic, cubic,... piecewise polynomials, respectively. An *open* knot vector has the first and the last knots repeated $p + 1$ times ensuring that the basis functions are interpolatory at the extrema of the parametric space [41]. In the following, we assume uniform, *i.e.*, equally spaced, open knot vectors.

The B-Spline basis functions $N_{i,p}$ can be defined starting with piecewise constants ($p = 0$) by means of a recursive formula

$$
N_{i,0} = \begin{cases} 1 & \text{if } \xi_i \leq \xi < \xi_{i+1} \\ 0 & \text{otherwise} \end{cases} \qquad i = 1, 2, ..., n
\tag{8}
$$

For $p = 1, 2, 3, \ldots$ it results:

$$
N_{i,p} = \begin{cases} \dfrac{\xi - \xi_i}{\xi_{i+p} - \xi_i} N_{i,p-1} + \dfrac{\xi_{i+p+1} - \xi}{\xi_{i+p+1} - \xi_{i+1}} N_{i+1,p-1}, & \text{if } \xi_i \leq \xi < \xi_{i+p+1} \\ 0, & \text{otherwise} \end{cases}
$$

Accordingly, basis functions of order p have $(p-1)$ continuous derivatives. If a knot is repeated k times, then the number of continuous derivatives decreases by k. A knot with multiplicity p, implies the basis functions to be interpolatory at that knot.

3.1. One Dimensional NURBS Interpolation

A non-uniform rational B-Spline in $\mathbb{R}^d$ is the projection onto d-dimensional physical space of a polynomial B-Spline defined in $(d+1)$-dimensional homogeneous coordinate space [41,42]. NURBS can be used to construct a vast gallery of geometrical entities, starting, for instance, from a discrete set of measured data [36]. The projective transformation of a B-Spline curve yields a rational polynomial curve. Inductively, the order p of a NURBS basis is identified as the order of the polynomial basis from which it was generated by projection.

A NURBS interpolation in $\mathbb{R}^d$ is constructed starting from a data set $\mathbf{B}_i^w$ $(i = 1, ..., n)$ or control points, for a B-Spline curve in $\mathbb{R}^{d+1}$ with knot vector Ξ. The control points for the NURBS curve are given by [41]:

$$(B_i)_k = \frac{(B_i^w)_k}{w_i} \quad k = 1, ..., d \tag{9}$$

where $(B_i)_k$ is the kth component of the vector B_i and $w_i = (B_i^w)_{d+1}$ is referred to as the ith weight. The NURBS basis functions of order p are then defined as:

$$R_{i,p}(\xi) = \frac{w_i N_{i,p}(\xi)}{\sum_{i=1}^n w_i N_{i,p}(\xi)} \tag{10}$$

Their first and second derivatives are given, respectively, by:

$$(R_{i,p})'(\xi) = \frac{w_i N'_{i,p}(\xi)}{\sum_{i=1}^n w_i N_{i,p}(\xi) w_i} - \frac{w_i N_{i,p}(\xi) N'_{i,p}(\xi) w_i}{\left(\sum_{i=1}^n w_i N_{i,p}(\xi)\right)^2} \tag{11}$$

and

$$\begin{aligned} (R_{i,p})''(\xi) = {} & \frac{w_i N''_{i,p}(\xi)}{\sum_{i=1}^n w_i N_{i,p}(\xi)} + \\ & + \frac{2 w_i N_{i,p}(\xi) \left(\sum_{i=1}^n w_i N'_{i,p}(\xi)\right)^2}{\left(\sum_{i=1}^n w_i N_{i,p}(\xi)\right)^3} + \\ & - \frac{2 w_i N'_{i,p}(\xi) \sum_{i=1}^n w_i N'_{i,p}(\xi) + w_i N_{i,p}(\xi) \sum_{i=1}^n w_i N''_{i,p}(\xi)}{\left(\sum_{i=1}^n w_i N_{i,p}(\xi)\right)^2} \end{aligned} \tag{12}$$

A pth degree NURBS curve is defined by:

$$\mathbf{C}(\xi) = \sum_{i=1}^n R_{i,p}(\xi) B_i \tag{13}$$

4. NURBS-Based Collocation Method

The main idea in the collocation method is to approximate the strong form of the equilibrium equations, without addressing a weak formulation typical of the finite element approach [8]. With reference to problem (6) or (7), the method consists in the approximation of the solution $\mathbf{u}^{(j)}$, $j = 0, 1, 2, ...$, as:

$$\tilde{\mathbf{u}}^{(j)} = \sum_{i=1}^n R_{i,p}(\xi) \tilde{\mathbf{u}}_i^{(j)} \tag{14}$$

where the interpolation functions $R_{i,p}(\xi)$ follow (10). The discrete form of (6)-(7) is thus obtained substituting (14) into the equilibrium operator $\mathcal{L}^{(j)}$ and into the boundary conditions operator $\mathcal{B}^{(j)}$, respectively. This leads to a set of $5n$ linear equations for the control values corresponding to (14). These unknown control values are obtained by enforcing the resulting discrete governing equations at n prescribed points in the parametric space, ξ_c ($c = 1, ..., n$), defined *collocation points*:

- Free vibration problem

$$
\begin{cases}
\mathcal{L}^{(j)}(\tilde{\mathbf{u}}^{(j)}(\xi_c)) = \left(\omega^{(j)}\right)^2 \mathcal{M}(\xi_c)(\tilde{\mathbf{u}}^{(j)}(\xi_c)) \,, & c = 2, ..., n-1 \\
\mathcal{B}^{(j)}(\tilde{\mathbf{u}}^{(j)}(\xi_c)) = \mathbf{0} \,, & c = 1, n
\end{cases}
\tag{15}
$$

- Static equilibrium problem

$$
\begin{cases}
\mathcal{L}^{(j)}(\tilde{\mathbf{u}}^{(j)}(\xi_c)) = \mathbf{q}(\xi_c) \,, & c = 2, ..., n-1 \\
\mathcal{B}^{(j)}(\tilde{\mathbf{u}}^{(j)}(\xi_c)) = \mathbf{0} \,, & c = 1, n
\end{cases}
\tag{16}
$$

Solution is thus obtained by solving for the unknown control values $\tilde{\mathbf{u}}_i^{(j)}$.

Collocation points are a set of natural coordinate values ξ_c, $c = 1, ..., n$, related to the knot vector. In the present case we will adopt the so called Greville nodes [36,43], *i.e.*,:

$$
\xi_c = \frac{1}{p} \sum_{k=c+1}^{c+p} \xi_k, \quad c = 1, ..., n
\tag{17}
$$

The choice for collocation points is generally guided by an accuracy/efficiency criterion. The idea is to have a set of points for which known solutions of certain differential operators are exactly recovered by the numerical scheme [17,44–46]. The choice for collocating governing equations as in Equation (17) has proved efficient in previous NURBS-based collocation approaches [8,32,33], as it grants high-order accuracy and smoothness of the parametrization of the unknown with excellent convergence properties. Noteworthy, according to Johnson [46], Greville collocation points are associated to the property of linear precision [43], in the sense that if these are used to compute a B-Spline approximation of a straight line of the form $l(u) = au + b$, the corresponding B-Spline curve is a straight line.

Given the interesting performance of standard Lagrange interpolation spaces, for the implementation of 1D collocation methods for shells of revolution, reported by previous researches [13–16], in what follows, we explore the superior accuracy of the NURBS approximation in conjunction with the collocation approach. The attractiveness of this approximation is twofold: (*i*) the NURBS high regularity suggests the possibility of obtaining smooth solutions even with low order approximation and low number of degrees of freedom, (*ii*) the capability of describing complex geometries is interesting especially from a structural design point of view, when constructing geometrical models from measured data is required.

The discretization and solution of problem Equations (6) or (7) is programmed as follows:

1. Define NURBS order p, number of control points n, build open knot vector Ξ, build NURBS basis and derivatives;
2. Compute collocation points ξ_c, $c = 1, 2, ..., n$;
3. Parametrize curvilinear space coordinate $z = [z_i, z_f]$ as $z = z(\xi)$, and relevant geometric quantities, *i.e.*, $R(z(\xi))$, $A_1(z(\xi))$, $\sin \phi(z(\xi))$;
4. Collocate above mentioned quantities at collocation points;
5. Approximate equilibrium, mass matrix, and boundary conditions operators: $\mathcal{L}^{(j)}(z(\xi))$, $\mathcal{M}(z(\xi))$, and $\mathcal{B}^{(j)}(z(\xi))$, respectively, and applied load distribution $\mathbf{q}^{(j)}(z(\xi))$, through NURBS interpolants;

6. Collocate discrete governing equations, *i.e.*, equilibrium [resp. boundary condition] equations at internal [resp. boundary] collocation points;
7. Assemble linear equations, viz. (15)-(16);
8. Solve for $\bar{\mathbf{u}}_i^{(j)}$, $j = 0, 1, ...$;
9. Post-process solution through NURBS interpolation.

As it is well known, such a discretization procedure does not lead to symmetric banded linear sets of equations as it is the case with finite element procedures. In particular, the coefficient matrix is sparse and nonsymmetric [44]; accordingly, factorization methods are generally not the most efficient, especially when dealing with large scale simulations. It is therefore recommended to resort to iterative methods such as conjugate gradient methods and residual based methods; is nonetheless noted that, albeit nonsymmetric, the pattern of coefficient matrices in displacement-based collocation approaches results competitive with respect to Galerkin finite element approaches which as known lead to symmetric systems [8].

5. Numerical Results

The present section is dedicated to numerical tests validating the NURBS collocation method for shells of revolution presented in the previous section. In subsection 5.1, we first present the asymptotic analysis of the fundamental eigenfrequency for shells of revolution of different Gaussian curvature (see (34)), an evidential benchmark test for assessing robustness with respect to membrane and shear locking in rotational shell numerical formulations. Secondly, we address the classical free vibration problem for different shells of revolution and different boundary conditions, comparing results with reference solutions. In subsection 5.2, a set of static problems are taken into consideration, in order to address the question of accuracy and convergence with respect to the order of interpolation and discretizaion. Finally, a simple technical problem is considered, validating the applicability of the present approach to problems of shell analysis and design, for shells with complex geometry.

5.1. Free Vibration Problems

5.1.1. Asymptotic Analysis of Fundamental Frequency

Following [47–49], in this section we study the dependence of the lowest (fundamental) frequency on the thickness t as this quantity approaches zero. Three representative cases of *Parabolic* (zero Gaussian curvature), *Elliptic* (positive Gaussian curvature), and *Hyperbolic* (negative Gaussian curvature) shells of revolution are considered. The shells have clamped boundary conditions, in order to study the inhibited pure bending behavior [49]. The three cases reported in the following are characterized, respectively, by meridian equation of:

- *Parabolic* shape:

$$R(z) = 1, \qquad z \in [-H, H] \tag{18}$$

- *Elliptic* shape:

$$R(z) = \sqrt{b^2 \left(1 - \frac{z^2}{a^2}\right)}, \qquad z \in [-H, H] \tag{19}$$

with $a^2 = \frac{25}{9}H^2$, $b^2 = H^2$;
- *Hyperbolic* shape:

$$R(z) = \sqrt{a^2 \left(1 + \frac{z^2}{b^2}\right)}, \qquad z \in [-H, H] \tag{20}$$

with $a^2 = H^2$, $b^2 = \frac{16}{9} H^2$.

and $H = 1$. Material constants for the numerical simulations are $E = 2.1 \times 10^{11}$ Pa, $\nu = 0.3$, $\rho = 7868$ Kg/m^3. The scope of this test is to check the asymptotic behaviors of the square of the fundamental, *i.e.*, lowest, eigenfrequency ω_0^2 when computed with the NURBS collocation method. In passing, it is recalled that the lowest eigenfrequency ω_0^2 does not necessarily correspond to harmonic number $j = 0$, nor any specific a-priori-known value j. Expected asymptotic rates are [47,50]:

- *Parabolic shell*:

$$\lim_{t \to 0} \omega_0^2 = t \tag{21}$$

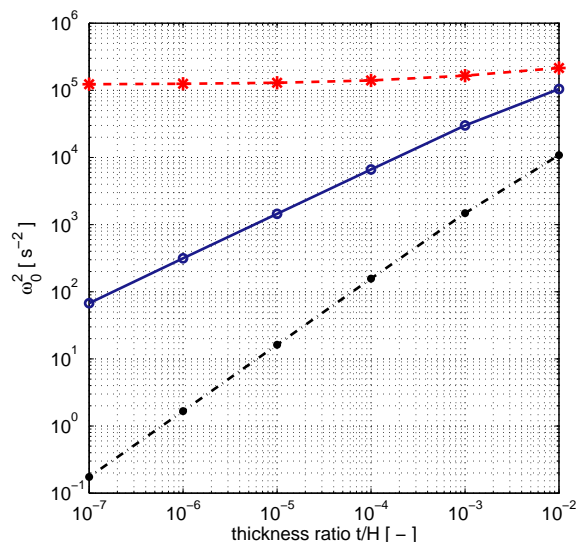- *Elliptic shell*:

$$\lim_{t \to 0} \omega_0^2 = t^0 \tag{22}$$

- *Hyperbolic shell*:

$$\lim_{t \to 0} \omega_0^2 = t^{2/3} \tag{23}$$

In Figure 2 we report the logarithmic dependence of ω_t^2 *vs.* thickness ratio t/H, for the three considered geometries. Accuracy in the low thickness range requires a fine discretization and high NURBS interpolation order, namely $n = 101$ and $p = 11$. In Table 1 we report the eigenvalues at specified thickness values, delimiting subsequent thickness branches in the logarithmic scale. The slopes of these branches are in agreement with the theoretical prediction on asymptotic behavior of the fundamental frequency Equations (21)–(23). The above results prove the present method is capable of efficient treatment of situations in which geometry, boundary conditions and regularity of applied loads induce a so called intermediate state for which nor the bending strain energy or the membrane strain energy dominates on one another in the asymptotic regime, and interior or boundary layers concentrate the majority of the strain energy. Such situations are prone to numerical locking and strong instabilities in the solution [34,48]. In this regard, a necessary condition for a numerical scheme to be locking-free is given by Equations (21)–(23), which are satisfied by the present method.

Figure 2. Asymptotic analysis of fundamental frequency. Asymptotic pattern of lowest eigenfrequency ω_0 with respect to thickness ratio t/H approaching zero. Different shells of revolution: *elliptic* - red dashed line with stars, *parabolic* - blue solid line with circles, *hyperbolic* - black dashed-dot line with bullets.

Table 1. Asymptotic analysis of fundamental frequency ω_0^2 with respect to thickness ratio t/H for *elliptic*, *parabolic*, and *hyperbolic* shells of revolution. Slope values for different branch values in the asymptotic regime.

| t/H	Parabolic	Slope	Elliptic	Slope	Hyperbolic	Slope
10^{-2}	104.215276		464.007232		323.741324	
		0.86531		0.11402		0.54346
10^{-3}	38.483324		406.921457		173.166457	
		0.97565		0.07091		0.65487
10^{-4}	12.515376		375.017756		81.474984	
		0.953114		0.03469		0.66104
10^{-5}	4.025786		360.333432		38.062875	
		0.98518		0.01484		0.66326
10^{-6}	1.289914		354.228976		17.736469	
		0.98857		0.00610		0.66686
10^{-7}	0.417654		351.74876		8.211765	

5.1.2. Clamped Hemispherical Shell in Free Vibration

A clamped hemispherical dome with radius a and uniform thickness t ($a/t = 100$), see Figure 3, is considered [51,52]. The values of the non-dimensional frequency parameter $\lambda = a\omega^{(j)}(\rho/E)^{1/2}$ are reported in Table 2, for the first six modes and for different values of the harmonic number j. Reference results obtained with a Lagrange collocation method [14], and those from a Spline finite element solution by Luah and Fan [53] are reported for validation. The present frequency parameter values are obtained selecting $n = 35$, $p = 4$ for the lowest mode frequencies, up to $n = 85$, $p = 8$ for higher modes. Noteworthy, the closed apex condition required by this type of shell [16,37] can be modeled by the present approach straightforwardly, as it implies enforcement of special homogeneous Dirichlet boundary condition at $z = 0$, depending on the harmonic number j:

$$u^{(0)} = v^{(0)} = \beta_1^{(0)} = \beta_2^{(0)} = 0 \tag{24}$$

$$u^{(1)} + v^{(1)} = 0, \quad w^{(1)} = 0, \quad \beta_1^{(1)} + \beta_2^{(1)} = 0 \tag{25}$$

$$u^{(j)} = v^{(j)} = w^{(j)} = \beta_1^{(j)} = \beta_2^{(j)} = 0, \quad j \geq 2 \tag{26}$$
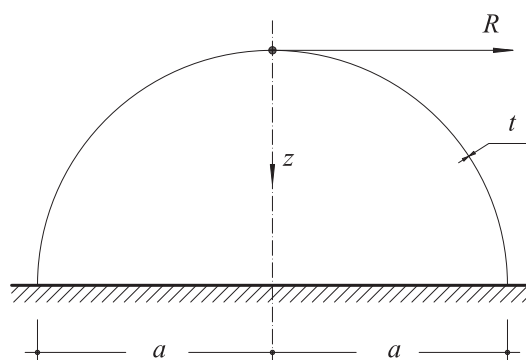
Figure 3. Clamped hemispherical shell in free vibration. Cross section.

The present results are in agreement with the reference results, confirming the accuracy of the proposed technique, even for cases in which shear locking is expectable [54]. The method proves computationally efficient as even in the higher mode regime, the size of the eigenvalue problem is smaller than that associated to the reference results.

5.1.3. Simply supported circular plate in free vibration

A circular plate of radius a and thickness t, simply supported along the boundary, is considered. For conciseness, we shall refer to the shell geometry and boundary conditions as shown in Figure 7 even if related to the numerical test reported in Section 5.2.2. The non-dimensional parameter $\lambda = [12(1 - \nu^2)\rho a^4(\omega^{(j)})^2/(Et^2)]^{1/2}$ computed with the present method is reported in Table 2, in agreement with reference values obtained in [14], and with those available from a Spline finite element approach by Luah and Fan [53]. The results confirm the interesting capabilities of the proposed approach for the free vibration analysis of rotational shells with different shapes and boundary conditions at a low computational cost. Numerical simulations show monotonic convergence to the computed eigenfrequencies, for increasing interpolation order p up to $p = 5$, and discretization order n up to $n = 35$. No spurious modes arise.
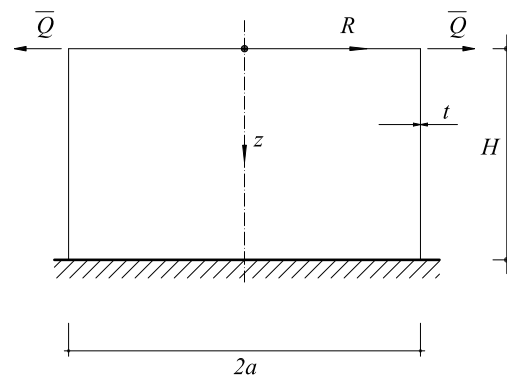

Figure 4. Cantilever cylindrical shell under tip load. Cross section.

Table 2. Clamped hemispherical shell in free vibration. Non-dimensional frequency parameter $\lambda = a\omega^{(j)}(\rho/E)^{1/2}$. Reference results from [53] (parentheses) and from [14] (brackets).

Harmonic Number j	Mode Number m					
	1	**2**	**3**	**4**	**5**	**6**
0	0.761 (0.761) [0.760]	0.939 (0.938) [0.938]	0.988 (0.984) [0.984]	1.029 (1.021) [1.020]	1.087 (1.021) [1.070]	1.172 (−) [1.146]
1	0.567 (0.567) [0.567]	0.893 (0.894) [0.893]	0.965 (0.966) [0.965]	1.003 (1.002) [1.002]	1.047 (1.046) [1.046]	1.112 (1.106) [1.115]
2	0.901 (0.901) [0.901]	0.966 (0.966) [0.966]	0.998 (0.998) [0.997]	1.030 (1.031) [1.029]	1.079 (1.081) [1.077]	1.151 (1.153) [1.150]
3	0.947 (0.948) [0.947]	0.989 (0.990) [0.988]	1.023 (1.024) [1.022]	1.065 (1.066) [1.063]	1.121 (1.124) [1.119]	1.203 (1.207) [1.206]
4	0.969 (0.969) [0.969]	1.005 (1.005) [1.004]	1.043 (1.045) [1.042]	1.094 (1.095) [1.091]	1.162 (1.167) [1.159]	1.259 (1.264) [1.266]
5	0.984 (0.985) [0.985]	1.020 (1.021) [1.019]	1.065 (1.066) [1.062]	1.124 (1.127) [1.120]	1.208 (1.213) [1.204]	1.321 (1.327) [1.341]

5.2. Static Equilibrium Problems

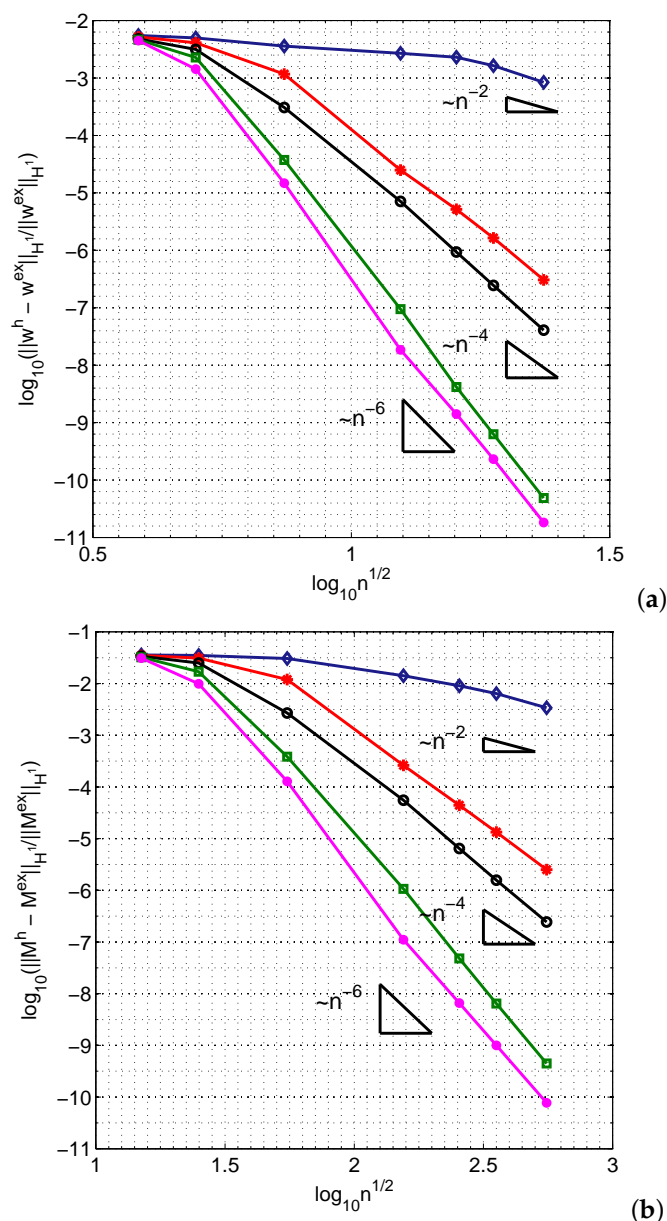### 5.2.1. Cantilever Cylindrical Shell under Tip Load

A circular cylindrical shell, clamped at one end, with a uniform radial line load $\bar{Q} = 1$ kN/m acting on the free edge, is considered, see Figure 4. The geometric data are $R = 5$ m, $t = 0.01$ m, $H = 6$ m, the Young's modulus and the Poisson ratio are, respectively, $E = 10^7$ kN/m^2, and $\nu = 0.3$. Axial symmetry permits to address the equilibrium problem for the $j = 0$ harmonic only. The line load is taken into account by modifying the free boundary conditions at $z = 0$, Equations (59)–(61), to guarantee that Q_{11} equals the applied force on that boundary.

The present classical benchmark is here adopted as a tool for calibrating the model with respect to parameters n and p, *i.e.*, mesh discretization ($h-$refinement) and order of interpolation ($p-$refinement), and for a given accuracy level. To this end, a reference solution proposed by Timoshenko and Woinowsky-Krieger [55] for semi-infinite circular cylindrical shells in axisymmetrical bending, is here taken into consideration for comparison and accuracy assessment. The structural behavior, which shifts from shear-flexural near the loaded edge to membrane dominated at the clamped boundary, is correctly reproduced by the NURBS-based collocation approach, as can be seen in Figure 5a,b, where M_{11} and Q_{11} are plotted, respectively, for an overkilling discretization with $n = 250$ and $p = 7$ with a relative error norm below 10^{-12}, together with values computed through the reference solution at selected locations. The results are in agreement, plus the static boundary condition is exactly satisfied in solution.
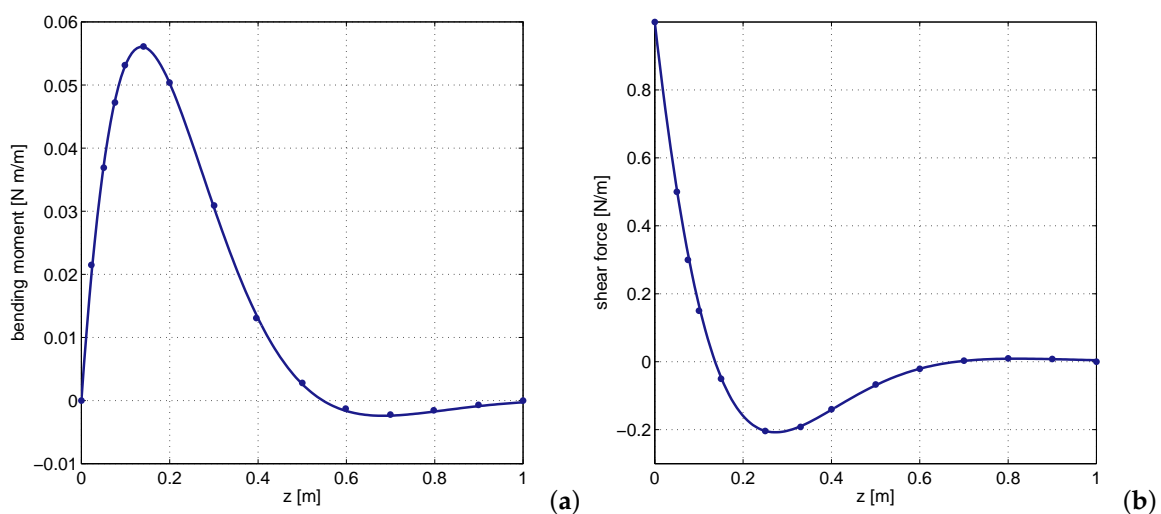
Figure 5. Cantilever cylindrical shell under tip load. (**a**) Bending moment M_{11}: blue solid line—present results *vs.* blue bullets—reference results [55]. (**b**) Shear force Q_{11}: blue solid line—present results *vs.* blue bullets—reference results [55].

Moreover, in order to assess the method convergence properties, we have plotted the H^1-error norms, of the tip transverse displacement $w(0)$, Figure 6a, and of bending moment $M_{11}(0)$, Figure 6b, for odd and even NURBS order p, and for increasing discretization refinements n. The asymptotic tendency of the error norm is consistent with analogous results reported in [31], where the static problem for Timoshenko spatial beams is addressed with a NURBS based collocation method. In particular, the logarithmic error is of the order n^{-p} for any duplets of orders $(p, p + 1)$, with even p, as theoretically predicted [32].

Figure 6. Cantilever cylindrical shell under tip load. Accuracy and convergence assessment for $h-$refinement and $p-$refinement. H^1-norm relative error $\log-\log$ plot for different on-Uniform Rational B-Spline (NURBS) interpolation order p and different discretization size n: (**a**) transverse tip displacement $w(0)$; (**b**) shear force $Q_{11}(0)$. blue diamonds - $p = 3$, red stars - $p = 4$, black circles - $p = 5$, green squares $p = 6$, magenta bullets $p = 7$.

5.2.2. Simply Supported Circular Plate Subject to Uniform Pressure

We consider a simply supported circular plate under uniform normal load q_w, Figure 7. This benchmark has a closed-form solution, cfr. [56]. The material parameters are $E = 10^6$ kN/m^2, $\nu = 0.0$, the plate radius is $a = 1$ m, the thickness is $t = 10^{-3}$ m, and the applied surface load is $q_w = 1$ kN/m^2. The load presents axial symmetry and requires to solve (7) for the $j = 0$ harmonic only; closed apex conditions plus straight meridian geometry is fully taken into account by the present approach as the former amounts to special homogeneous Dirichlet boundary conditions (24), the latter is contemplated by (30)-(31). We report in Table 4 the results obtained with the present approach, compared with an analytical solution [37], and with a hybrid mixed rotational finite element solution [57]. A space discretization characterized by $n = 7$ and $p = 4$ is sufficient to obtain accurate results. Resorting to

the NURBS basis structure, post-processed quantities such as the bending and twisting moments in Figure 8a, and the rotation degrees of freedom in Figure 8b, can be plotted.
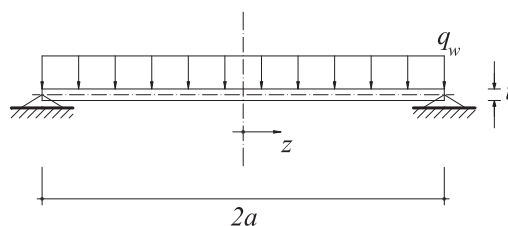

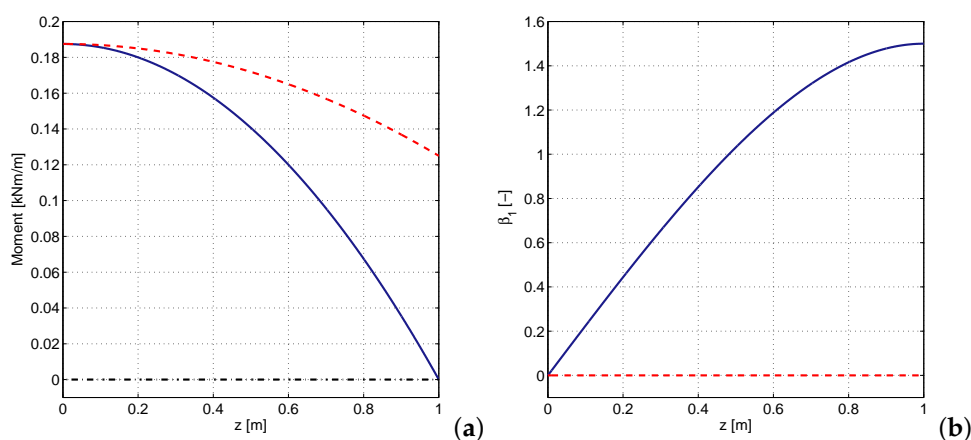**Figure 7.** Simply supported circular plate subject to uniform pressure. Cross section.

Figure 8. Simply supported circular plate subject to uniform pressure q_w. (**a**) Bending moment M_{11} - blue solid line, bending moment M_{22} - red dotted line), twisting moment M_{12} - black dashed-dot line; (**b**) Rotation β_1 - blue solid line, rotation β_2 - red dotted line.

Table 3. Simply supported circular plate in free vibration. Frequency parameter $\lambda = [12(1 - \nu^2)\rho a^4 (\omega^{(j)})^2 / (Et^2)]^{1/2}$. Reference results from [14] (parentheses) and from [53] (brackets).

Harmonic Number n	Maude Number m					
	1	2	3	4	5	6
	4.93542	29.7232	74.171	138.356	222.303	325.953
0	(4.93515)	(29.7201)	(74.1553)	(138.324)	(222.164)	(324.896)
	[4.93515]	[29.7301]	[74.1576]	[138.329]	[224.264]	[326.013]
	13.8981	48.4784	102.771	176.794	270.551	384.048
1	(13.6586)	(49.9285)	(102.909)	(178.803)	(270.489)	(384.078)
	[13.8982]	[48.4791]	[102.776]	[176.816]	[270.630]	[384.279]
	25.6131	70.1160	134.295	218.209	321.919	445.651
2	(25.6132)	(70.1163)	(134.295)	(218.195)	(321.826)	(445.187)
	[25.6128]	[70.1150]	[134.296]	[218.213]	[321.909]	[445.467]
	39.9569	94.5470	168.668	262.470	375.990	509.272
3	(39.9570)	(94.5476)	(168.670)	(262.474)	(375.991)	(509.231)
	[39.9573]	[95.5496]	[168.681]	[262.519]	[376.142]	[509.661]
	56.8408	121.699	205.841	309.588	433.026	576.244
4	(56.8411)	(121.700)	(205.845)	(309.593)	(433.021)	(576.155)
	[56.8416]	[121.703]	[205.859]	[309.649]	[433.205]	[576.673]
	76.2018	151.513	245.765	359.507	492.896	646.089
5	(76.2022)	(151.514)	(245.769)	(359.513)	(492.884)	(645.932)
	[76.2031]	[151.519]	[245.787]	[359.581]	[493.104]	[646.548]

Table 4. Simply supported circular plate subject to uniform pressure. Comparison of present results for w, β_1, and M_{11} at different locations z, for $cp = 7$, $p = 4$. Theoretical results from [56], reference results from [57].

|	z [m]	Theor. [56]	Present	Ref. [57]
	0.00	0.938	0.938	0.939
	0.25	0.868	0.868	0.868
$w \times 10^{-3}$ [m]	0.50	0.668	0.668	0.668
	0.75	0.364	0.364	0.364
	1.00	0	0	0
	0.00	0	0	0
	0.25	0.551	0.551	0.551
$\beta_1 \times 10^{-3}$	0.50	1.031	1.031	1.031
	0.75	1.371	1.371	1.371
	1.00	1.500	1.500	1.500
	0.00	0.188	0.188	0.188
	0.25	0.176	0.176	0.176
M_{11} [kN m/m]	0.50	0.141	0.141	0.141
	0.75	0.082	0.082	0.082
	1.00	0	0	3×10^{-14}

5.2.3. Hemispherical Shell under Uniform Pressure

This numerical test presents a spherical shell of radius $a = 1$ and uniform thickness $t = 0.01$, see Figure 9. The shell is loaded by a uniform internal pressure $q_w = 1$. The Young modulus is $E = 2.1 \times 10^{11}$ and the Poisson ratio is $\nu = 0.3$. Due to symmetry, only the upper half shell is modeled, with closed apex conditions at $z = 0$ and sliding edge boundary condition at $z = R$. The solution for displacement and strain components is expected to in a pure membrane dominated regime with zero shear/bending deformation. Henceforth, given the aim of the present test, no reference solution is here taken into account. The NURBS collocation is applied with $n = 35$ and $p = 5$, sufficient to grant the exact solution reported in the following. The results shown in Figure 10a,b for displacement and strain components are in agreement with theory, in particular zero tangential displacements v as well as null membrane shearing strains ε_{12} are correctly recovered, for a pure membrane equilibrium state of the spherical shell characterized by $\varepsilon_{11} = \varepsilon_{22}$. It is readily checked that curvature variations and shear strains are identically zero as expected.
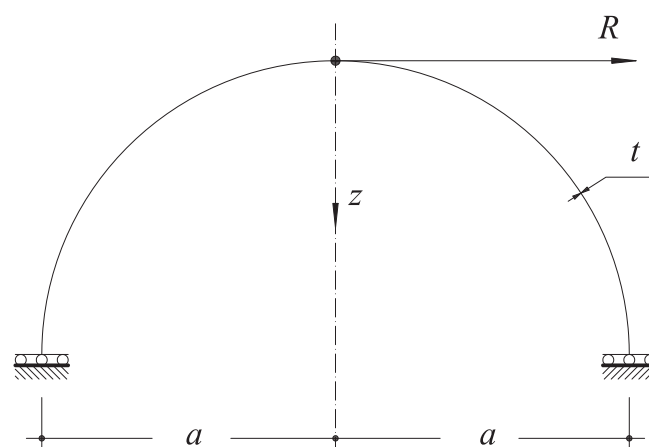
Figure 9. Hemispherical shell under uniform pressure. Cross section.
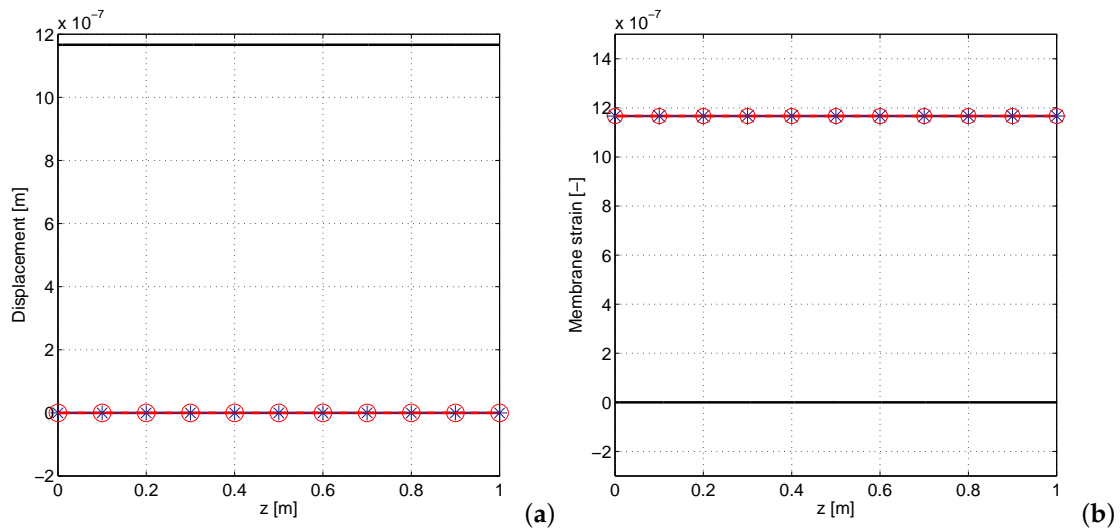
Figure 10. Spherical shell under uniform pressure. (**a**) Displacement components: u - blue solid line with stars, v - red dotted line with circles, w - black solid line. (**b**) Strain components: ε_{11} - blue solid line with stars, ε_{22} - red dotted line with circles, ε_{12} - black solid line.

5.2.4. Hyperboloid of Revolution under Wind Load

The example presents a doubly curved hyperboloid of revolution, a typical cooling tower structure, Figure 11, subject to wind pressure. Geometrical data for the shell are, $a = 84$ ft, $T = 60$ ft, $H = 330$ ft, $t = 7$ in. The Young modulus is $E = 432 \times 10^6$ lb/ft^2, Poisson ratio is $\nu = 0.15$. The surface load q_w is constant along the tower height, and is not symmetric with respect to the axis of revolution; in particular, q_w varies with the circumferential coordinate θ as reported in Figure 12 [57]. The distributed load is expanded in Fourier series taking into account the first ten harmonic components $j = 0, 1, ..., 9$. The present analysis aims at determining both displacements and stress resultants for the structure, which are respectively plotted in Figures 13 and 14, where a comparison with different reference solutions available in the literature is carried out [58], together with a reference solution computed with SHORE III, a ring finite element code developed by [59]. The proposed methodology yields reliable results for $n = 35$ and $p = 8$ even for the case of a doubly curved rotational shell with unsymmetrical loading, which produces complex stress resultants and couples patterns. The numerical test confirms the present method capability of analyzing real shell structures under complex loading conditions with favorable accuracy.
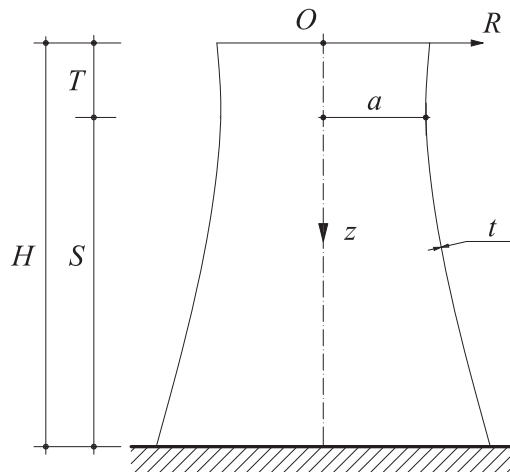
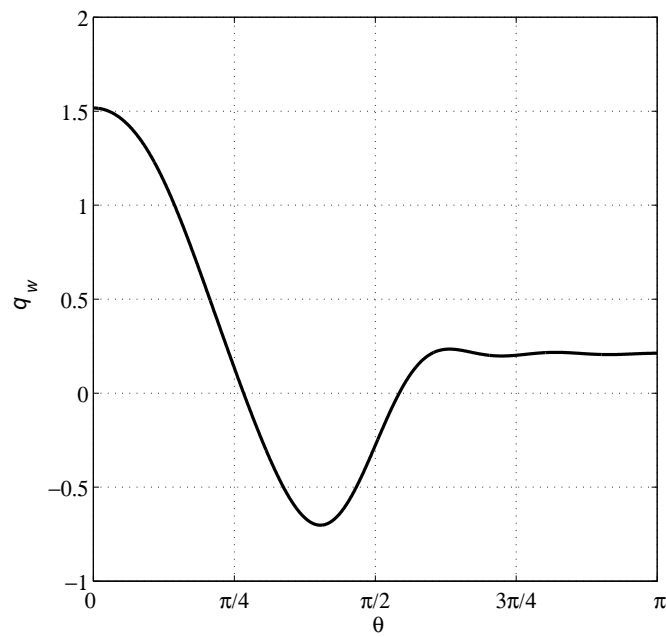**Figure 11.** Hyperboloid of revolution under wind load. Cross section.

Figure 12. Hyperboloid of revolution under wind load. Wind pressure q_w *vs.* circumferential angle θ.
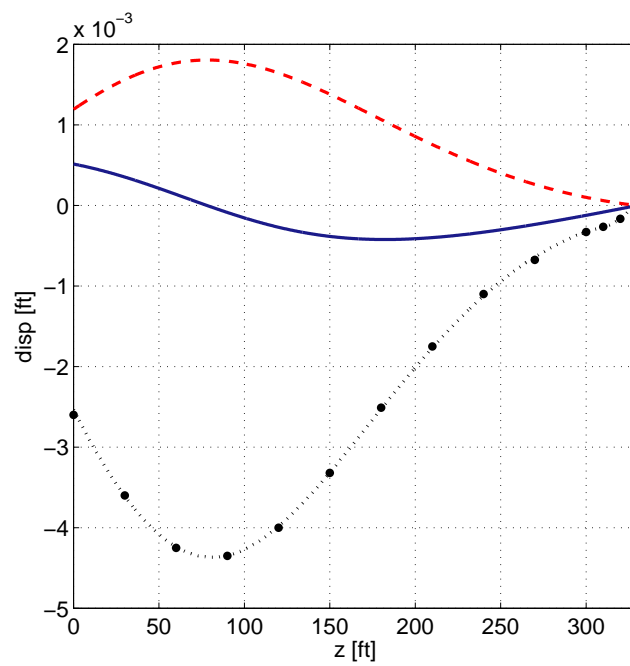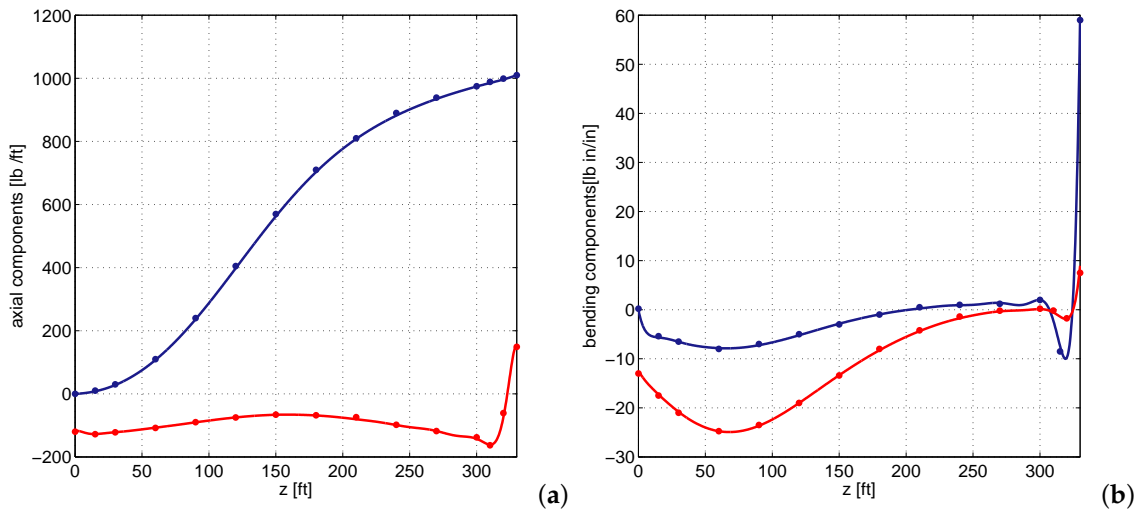

Figure 13. Hyperboloid of revolution under wind load. Displacement components: u—blue solid line, v—red dotted line, w black dashed-dotted line - present results *vs.* black bullets— reference results [58].

Figure 14. Hyperboloid of revolution under wind load. (**a**) Membrane stress resultant N_{11}: blue solid line—present approach *vs.* blue bullets—reference results [58]; membrane stress resultant N_{22}: red solid line - present approach *vs.* red bullets—reference results [58]. (**b**) Bending moment M_{11}: blue solid line—present approach *vs.* blue bullets—reference results [59]; bending moment M_{22}: red solid line - present approach *vs.* red bullets—reference results [59].

5.2.5. Torispherical tank subject to uniform internal pressure

The example presents a technical problem for a so called compound shell, namely a shell of revolution obtained by the smooth blending of different shell segments, each having a particular meridian curve geometry [37], see Figure 15. The shell comprises a closed-apex spherical cap OA_1 of radius $a_1 = 172.8981$ in. and length $H_1 = 18.675$ in., a torus segment $A_1 A_2$ of radius $a_2 = 32.74$ in. and length $H_2 = 29.2$ in., and a cylindrical portion with radius $a_3 = 96.1$ in. and length $H_3 = 24$ in.; the thickness t is uniformly equal to 0.20 in. The Young modulus is $E = 3.0 \times 10^4$ psi, the Poisson ratio is $\nu = 0.3$.
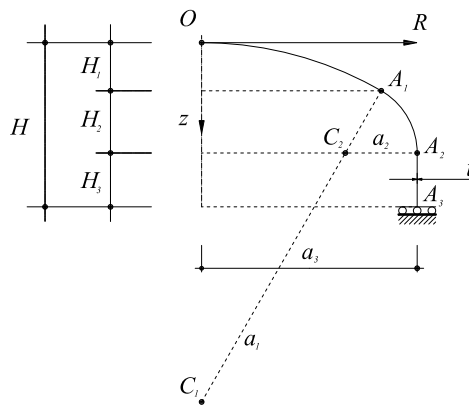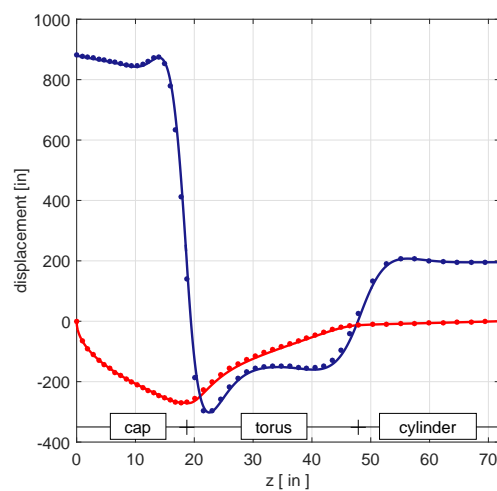

Figure 15. Torispherical tank subject to uniform internal pressure. Cross section.

In order to model the pre-buckling elastic stress pattern, which is known to induce particularly severe compressive circumferential stresses in the toroidal region, the shell is loaded by a uniform internal pressure $q_w = 150$ psi [37]. The geometry in the present analysis is constructed using three different NURBS control polygons, each one pertaining to a single shell segment, and each set with an equal number of basis functions. The three subdomains are then patched together, granting regularity of the meridian at the junctions and C^0 continuity of displacements and rotations, a procedure referred to as domain decomposition [44,45]. Nonetheless, it is pointed out that it is possible to use a single basis

to describe the entire geometry and to collocate governing equations over the single control polygon. NURBS basis for collocation is characterized by $n = 55$ on the spherical and toroidal segments, and $n = 7$ on the cylindrical region. The order of the interpolants is $p = 5$. The reference solution for this benchmark is provided by the finite element code SHORE III, adopting a fine mesh discretization with 128 quartic displacement based elements on both spherical and toroidal parts, and with 8 elements on the cylindrical segment. Results and comparison are plotted in Figure 16, reporting displacements u and w, and in Figure 17 for rotation β_1. Figure 18a [resp. 18b] show the axial σ_{11} and circumferential σ_{22} normal stress components at inner ($\zeta = -t/2$) and outer ($\zeta = t/2$) surface of the shell [60]:

$$\sigma_{ii} = \frac{N_{ii}}{t} \pm \frac{6M_{ii}}{t^2} \quad i = 1, 2 \tag{27}$$

obtained by post processing of stress resultants and couples. Remarkably good agreement is observed between present and reference results, confirming the capability of the proposed technique to study complex technically relevant problems for shells of revolution, as the aforementioned pre-buckling analysis of a cylindrical tank with torispherical head.

Figure 16. Torispherical tank subject to uniform internal pressure. Displacement components: u blue solid line - present approach *vs.* blue bullets - reference solution [53], w red solid line - present approach *vs.* red bullets - reference solution [59].
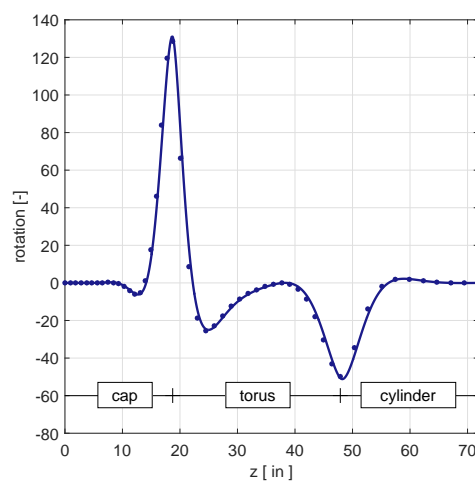
Figure 17. Torispherical tank subject to uniform internal pressure. Rotation β_1 solid blue line - present approach *vs.* blue bullets - reference solution [59].
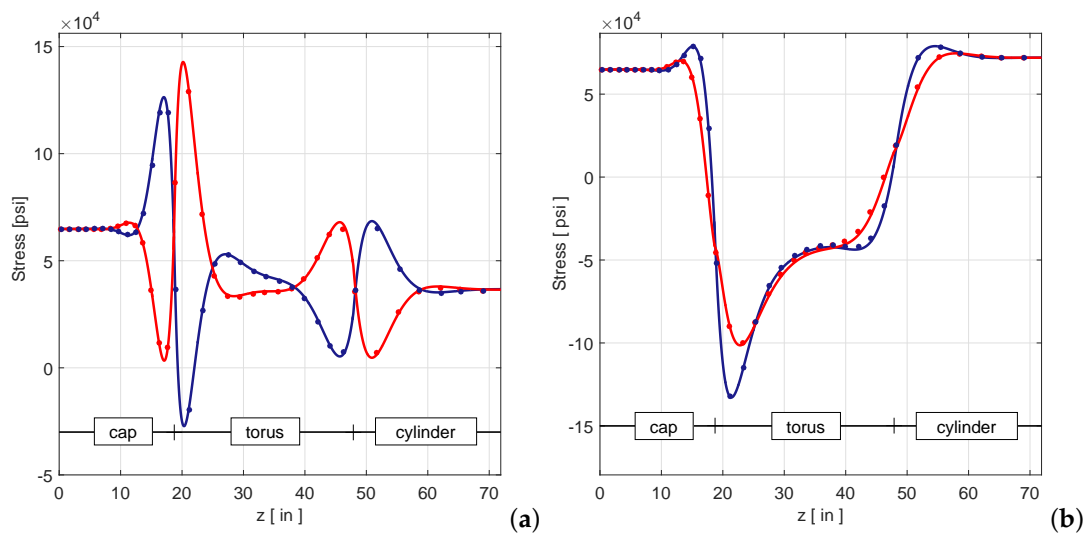
Figure 18. Torispherical tank subject to uniform internal pressure. (**a**) Axial normal stress σ_{11}—inner ($\zeta = -t/2$) blue solid line -present approach *vs.* blue bullets— reference solution [59], outer ($\zeta = t/2$) red solid line—present approach *vs.* red bullets—reference solution [59]. (**b**) Circumferential normal stress σ_{22}—inner ($\zeta = -t/2$) blue solid line—present approach *vs.* blue bullets— reference solution [59], outer ($\zeta = t/2$) red solid line - present approach *vs.* red bullets—reference solution [59].

6. Conclusions

In this paper we have presented a NURBS-based collocation method for the elastic analysis of shells of revolution. Both the free vibration and the static equilibrium problems have been investigated in the realm of Reissner-Mindlin theory. Use of Fourier series expansion of dependent variables with respect to the circumferential angle permits to solve the problem as a series of one-dimensional differential equation sets. A NURBS-based collocation method has been presented exploiting the superior behavior of such interpolation methodology which grants higher order accuracy and regularity. The proposed method has been tested on different free vibration and static equilibrium benchmark problems, showing its versatility and accuracy in computing free vibration modes and frequencies, as well as stresses and displacement patterns. Comparison with existing results seems encouraging and confirm the interesting approximation properties of NURBS basis functions which grant avoidance of numerical problems such as locking and instability. The robustness shown by the proposed methodology suggests implementation into a general purpose code for the structural analysis and design of complex shell structures.

Author Contributions: M.L.D.B. and E.A. equally contributed to modeling and numerical campaign in the present work.

Conflicts of Interest: The authors declare no conflict of interest.

Appendix A. Fundamental Relationships for Shells of Revolution

For later convenience, we introduce the diagonal matrix operators:

$$\tilde{D}_1^{(j)}(\theta) = \operatorname{diag}\left\{\cos j\theta, \sin j\theta, \cos j\theta, \cos j\theta, \sin j\theta\right\}, \tag{28}$$

$$\tilde{D}_2^{(j)}(\theta) = \operatorname{diag}\left\{\cos j\theta, \cos j\theta, \sin j\theta, \cos j\theta, \cos j\theta, \sin j\theta, \cos j\theta, \sin j\theta\right\}, \tag{29}$$

$$j = 0, 1, 2, \ldots$$

Appendix A.1. Metric Quantities on Shell Mid-Surface

Given the meridian equation $R = R(z)$, the first fundamental form for shells of revolutions and the principal curvature radii of meridian read [37]:

$$A_1 = A_1(z) = [1 + (R_{,z})^2]^{1/2} \tag{30}$$

$$R_1(z) = -[1 + (R_{,z})^2]^{3/2}/(R_{,zz}) \tag{31}$$

$$R_2(z) = R(z)/\sin\phi(z) \tag{32}$$

where the sinus of colatitude angle ϕ (cfr. Figure 1) is given by:

$$\sin\phi(z) = [1 + (R_{,z})^2]^{-1/2} \tag{33}$$

The *Gaussian* curvature of the meridian is defined by:

$$\kappa(z) = \frac{1}{R_1(z)R_2(z)} \tag{34}$$

Appendix A.2. Fourier Series Expansions

Fourier series expansions with respect to the circumferential coordinate θ, for quantities relevant to the problem under consideration, are reported in the following:

- Displacements and rotations.

$$\mathbf{u}(z,\theta) = \sum_{n=0}^{\infty} \tilde{D}_1^{(j)}(\theta)\mathbf{u}^{(j)}(z) \tag{35}$$

with the vector

$$\mathbf{u}^{(j)}(z) = \left[u^{(j)}\ v^{(j)}\ w^{(j)}\ \beta_1^{(j)}\ \beta_2^{(j)} \right]^T \tag{36}$$

collecting the 5 displacement components harmonic amplitudes.

In the case of a free vibration problem, harmonic motion is assumed, *i.e.*, the time dependence of $\mathbf{u}^{(j)}(z,\tau)$ is taken as:

$$\mathbf{u}^{(j)}(z,\tau) = \mathbf{u}^{(j)}(z)\exp[-\mathrm{i}\omega^{(j)}\tau]$$

- Stress resultants and couples.

$$\mathbf{S}(z,\theta) = \sum_{n=0}^{\infty} \tilde{D}_2^{(j)}(\theta)\mathbf{S}^{(j)}(z) \tag{37}$$

with the vector

$$\mathbf{S}^{(j)}(z) = \left[N_{11}^{(j)}\ N_{22}^{(j)}\ N_{12}^{(j)}\ M_{11}^{(j)}\ M_{22}^{(j)}\ M_{12}^{(j)}\ Q_{11}^{(j)}\ Q_{22}^{(j)} \right]^T \tag{38}$$

collecting the 8 stress resultants harmonic amplitudes.

- Strain components.

$$\boldsymbol{\varepsilon}(z,\theta) = \sum_{n=0}^{\infty} \tilde{D}_2^{(j)}(\theta)\boldsymbol{\varepsilon}^{(j)}(z) \tag{39}$$

with the vector

$$\boldsymbol{\varepsilon}^{(j)}(z) = \left[\varepsilon_{11}^{(j)} \ \varepsilon_{22}^{(j)} \ \varepsilon_{12}^{(j)} \ \kappa_{11}^{(j)} \ \kappa_{22}^{(j)} \ \kappa_{12}^{(j)} \ \chi_{11}^{(j)} \ \chi_{22}^{(j)} \right] \tag{40}$$

ordering the 8 strain components harmonic amplitudes.

- Surface loads.

$$\mathbf{q}(z,\theta) = \sum_{n=0}^{\infty} \tilde{D}_1^{(j)}(\theta)\mathbf{q}^{(j)}(z) \tag{41}$$

with $\mathbf{q}^{(j)}(z) = \left[q_u^{(j)} \ q_v^{(j)} \ q_w^{(j)} \ 0 \ 0 \right]$.

Appendix A.3. Strain-Displacement Operator

Strain-displacement relationships, viz. Equation (5), are defined in Fourier series form, through the linear differential (8-row by 5-column) matrix operator $\mathcal{A}^{(j)}$ which gives the 8 strain components harmonic amplitudes $\boldsymbol{\varepsilon}^{(j)}(z)$, viz. Equation (40) in terms of the 5 displacement components harmonic amplitudes $\mathbf{u}^{(j)}(z)$, viz. Equation (36):

$$\boldsymbol{\varepsilon}^{(j)} = \mathcal{A}^{(j)}\mathbf{u}^{(j)} \tag{42}$$

whose non-null components turn out to be:

$$\mathcal{A}_{11}^{(j)} = (1/A_1)(\ldots)_{,z} \,; \mathcal{A}_{13}^{(j)} = (1/R)_1(\ldots) \tag{43}$$

$$\mathcal{A}_{21}^{(j)} = (R_{,z}/RA_1)(\ldots) \,; \mathcal{A}_{22}^{(j)} = (j/R)(\ldots) \,; \mathcal{A}_{23}^{(j)} = (\sin\phi/R)(\ldots) \tag{44}$$

$$\mathcal{A}_{31}^{(j)} = -(j/R)(\ldots) \,; \mathcal{A}_{32}^{(j)} = (R_{,z}/RA_1)(\ldots) + (1/A_1)(\ldots)_{,z} \tag{45}$$

$$\mathcal{A}_{44}^{(j)} = (1/A_1)(\ldots) \tag{46}$$

$$\mathcal{A}_{54}^{(j)} = (R_{,z}/RA_1)(\ldots) \,; \mathcal{A}_{55}^{(j)} = (j/R)(\ldots) \tag{47}$$

$$\mathcal{A}_{64}^{(j)} = -(j/2R)(\ldots) \,; \mathcal{A}_{65}^{(j)} = -(R_{,z}/2RA_1)(\ldots) + (1/2A_1)(\ldots)_{,z} \tag{48}$$

$$\mathcal{A}_{71}^{(j)} = -(1/R_1)(\ldots) \,; \mathcal{A}_{73}^{(j)} = (1/A_1)(\ldots)_{,z} \,; \mathcal{A}_{74}^{(j)} = (\ldots) \tag{49}$$

$$\mathcal{A}_{82}^{(j)} = -(\sin\phi/R)(\ldots) \,; \mathcal{A}_{83}^{(j)} = -(j/R)(\ldots) \,; \mathcal{A}_{85}^{(j)} = (\ldots) \tag{50}$$

for $j = 0, 1, 2, \ldots$. The entries of differential operator $\mathcal{A}^{(j)}$ are of the form: $\mathcal{A}_{lm}^{(j)} = f(z)(\ldots) + g(z)(\ldots)_{,z}$ ($l = 1, \ldots, 8; \ m = 1, \ldots, 5$), which represents the contribution to the $l-th$ component of $\boldsymbol{\varepsilon}^{(j)}(z)$ Equation (40) from the $m-th$ component of $\mathbf{u}^{(j)}(z)$ Equation (36). In particular, the term $f(z)(\ldots)$ stands for pre-multiplication of the function $f(z)$ by the $m-th$ component of $\mathbf{u}^{(j)}(z)$; the term $g(z)(\ldots)_{,z}$ stands for pre-multiplication of the function $g(z)$ by the first derivative of the $m-th$ component of $\mathbf{u}^{(j)}(z)$ with respect to z.

Appendix A.4. Linear Elastic Constitutive Equation

For linear elastic isotropic material, with Young's modulus E, and Poisson ratio ν, the constitutive equation relating internal action and strain components in Fourier series form, reads [37,38]:

$$\mathbf{S}^{(j)}(z) = \mathbb{C}\boldsymbol{\varepsilon}^{(j)}(z), \quad j = 0, 1, \ldots \tag{51}$$

being:

$$\mathbb{C} = \text{diag}\left\{\mathbb{C}_m, \mathbb{C}_b, \mathbb{C}_s\right\} \tag{52}$$

The constitutive matrix operator $\mathbb{C}$ is given by:

$$\mathbb{C}_m = \begin{bmatrix} E_1 & E_2 & 0 \\ E_2 & E_1 & 0 \\ 0 & 0 & E_3 \end{bmatrix} \; ; \; \mathbb{C}_b = \frac{t^2}{6}\mathbb{C}_m \; ; \; \mathbb{C}_s = \begin{bmatrix} E_7 & 0 \\ 0 & E_7 \end{bmatrix} \tag{53}$$

where $E_1 = Et/2(1-v^2)$, $E_2 = vE_1$, $E_3 = (1-v)E_1/2$, and $E_7 = (5/6)E_3$.

Appendix B. Equilibrium and Boundary Conditions Operators

Appendix B.1. Equilibrium Operator

With reference to Equations (6) and (7), the equilibrium operator $\mathcal{L}^{(j)}$ is defined as follows:

$$
\begin{aligned}
\mathcal{L}_{11}^{(j)} = 1/[R(1+R_{,z}^2)]\{&E_1 R_{,z}^2/R \\
&+ E_2 R_{,zz}[R_{,z}^2/(1+R_{,z}^2) - 1] \\
&+ j^2 E_3/R(1+R_{,z}^2) + E_7 R/R_1^2(1+R_{,z}^2)\}(...) \\
&+ E_1 R_{,z}/[R(1+R_{,z}^2)][(RR_{,zz})/(1+R_{,z}^2) - 1](...)_{,z} \\
&- E_1/(1+R_{,z}^2)(...)_{,zz}
\end{aligned}
$$

$$
\begin{aligned}
\mathcal{L}_{12}^{(j)} = jR_{,z}/[R^2(1+R_{,z}^2)^{1/2}]&(E_1+E_3)(...) \\
&- j(E_1+E_2)/[R(1+R_{,z}^2)^{1/2}](...)_{,z}
\end{aligned}
$$

$$
\begin{aligned}
\mathcal{L}_{13}^{(j)} = 1/[R(1+R_{,z}^2)^{1/2}]\{&E_1 R_{,z}/R[1/(1+R_{,z}^2)^{1/2} \\
&- R/R_1 - R^2/R_{,z}(1/R_1)_{,z}]\} \\
&+ E_2 R_{,z}[1/R_1 + R_{,zz}/(1+R_{,z}^2)^{3/2}]\}(...) \\
&+ 1/[R(1+R_{,z}^2)^{1/2}][-R/R_1(E_1+E_7) \\
&+ E_2/(1+R_{,z}^2)^{1/2}](...)_{,z}
\end{aligned}
$$

$$\mathcal{L}_{14}^{(j)} = -E_7/R_1(...)$$

$$\mathcal{L}_{15}^{(j)} = 0$$

$$
\begin{aligned}
\mathcal{L}_{21}^{(j)} = jR_{,z}/[R^2(1+R_{,z}^2)^{1/2}]&(E_1+E_3)(...) \\
&+ j(E_2+E_3)/[R(1+R_{,z}^2)^{1/2}](...)_{,z}
\end{aligned}
$$

$$
\begin{aligned}
\mathcal{L}_{22}^{(j)} = 1/[R^2(1+R_{,z}^2)][&E_1 j^2(1+R_{,z}^2)/R \\
&+ E_3 R R_{,z}^2 R_{,zz}(1/(1+R_{,z}^2)^{1/2} + 1/(RR_{,zz}) - 1) \\
&+ E_7](...) \\
&+ E_3 R_{,z}/[R(1+R_{,z}^2)](RR_{,zz}/(1+R_{,z}^2) - 1)(...)_{,z} \\
&- E_3/(1+R_{,z}^2)(...)_{,zz}
\end{aligned}
$$

$$
\begin{aligned}
\mathcal{L}_{23}^{(j)} = j/[R^2(1+R_{,z}^2)^{1/2}][&E_1 \\
&+ E_2 R(1+R_{,z}^2)^{1/2}/R_1 + E_7](...)
\end{aligned}
$$

$$\mathcal{L}_{24}^{(j)} = 0$$

$$\mathcal{L}_{25}^{(j)} = E_7/[R(1+R_{,z}^2)^{1/2}](...)$$

$$\mathcal{L}_{31}^{(j)} = 1/[R(1+R_{,z}^2)^{1/2}][E_1 R_{,z}/[R(1+R_{,z}^2)^{1/2}]$$
$$+ E_2/R_1 + E_7/R_{1,z}(R - R_{,z})](\ldots)$$
$$+ 1/[R(1+R_{,z}^2)^{1/2}][E_1/(RR_1) + E_2/(1+R_{,z}^2)^{1/2}$$
$$+ E_7 R/R_1](\ldots)_{,z}$$

$$\mathcal{L}_{32}^{(j)} = j/[R(1+R_{,z}^2)^{1/2}][E_1 + E_2(1+R_{,z}^2)^{1/2}/R_1$$
$$+ E_7/R](\ldots)$$

$$\mathcal{L}_{33}^{(j)} = [E_1(1/R^2 + 1/[R^2(1+R_{,z}^2)^{1/2}])$$
$$+ E_2(R_1/[R(1+R_{,z}^2)^{1/2}]$$
$$+ 1/[R_1 R(1+R_{,z}^2)^{1/2}]) + E_7 j^2](\ldots)$$
$$+ E_7 R_{,z}/[R(1+R_{,z}^2)][1 - RR_{,zz}/(1+R_{,z}^2)](\ldots)_{,z}$$
$$- E_7/(1+R_{,z}^2)(\ldots)_{,zz}$$

$$\mathcal{L}_{34}^{(j)} = -E_7 R_{,z}/[R(1+R_{,z}^2)]^{1/2}(\ldots)$$
$$- E_7/[R(1+R_{,z}^2)]^{1/2}(\ldots)_{,z}$$

$$\mathcal{L}_{35}^{(j)} = -jE_7/R(\ldots)$$

$$\mathcal{L}_{41}^{(j)} = -E_7/R_1(\ldots)$$

$$\mathcal{L}_{42}^{(j)} = 0$$

$$\mathcal{L}_{43}^{(j)} = E_7/(1+R_{,z}^2)^{1/2}(\ldots)_{,z}$$

$$\mathcal{L}_{44}^{(j)} = 1/[R(1+R_{,z}^2)]\{E_4 R_{,z}^2/R$$
$$+ E_5 R_{,z}^2[1/(1+R_{,z}^2) - 1] + j^2 E_6/R(1+R_{,z}^2)$$
$$+ E_7 R(1+R_{,z}^2)\}(\ldots)$$
$$+ 1/[R(1+R_{,z}^2)^2][E_4 R_{,z}(RR_{,zz}/(1+R_{,z}^2) - 1)](\ldots)_{,z}$$
$$- E_4/(1+R_{,z}^2)(\ldots)_{,zz}$$

$$\mathcal{L}_{45}^{(j)} = jR_{,z}/[R^2(1+R_{,z}^2)^{1/2}][E_4 + E_6](\ldots)$$
$$- j/[R(1+R_{,z}^2)^{1/2}](E_5 + E_6 R)(\ldots)_{,z}$$

$$\mathcal{L}_{51}^{(j)} = 0$$

$$\mathcal{L}_{52}^{(j)} = -E_7/[R(1+R_{,z}^2)^{1/2}]$$

$$\mathcal{L}_{53}^{(j)} = -jE_7/R$$

$$\mathcal{L}_{54}^{(j)} = jR_{,z}/[R^2(1+R_{,z}^2)^2](E_4 + E_6)(\ldots)$$
$$+ j/[R(1+R_{,z}^2)^2](E_5 + E_6)(\ldots)_{,z}$$

$$\mathcal{L}_{55}^{(j)} = 1/[R(1+R_{,z}^2)][E_4 j^2(1+R_{,z}^2)/R$$
$$+ E_6 R_{,zz}(1 - R_{,z}^2/(1+R_{,z}^2) + R_{,z}^2/(RR_{,zz}))$$
$$+ E_7 R(1+R_{,z}^2)](\ldots)$$
$$+ 1/[R(1+R_{,z}^2)][E_6 R_{,z}(RR_{,zz}/(1+R_{,z}^2) - 1)](\ldots)_{,z}$$
$$- E_6/(1+R_{,z}^2)(\ldots)_{,zz}$$

The entries of differential operator $\mathcal{L}^{(j)}$ are of the form: $\mathcal{L}^{(j)}_{lm} = f(z)(...) + g(z)(...)_{,z} + +h(z)(...)_{,zz}$ ($l = 1, ..., 5$; $m = 1, ..., 5$), which represents the contribution to the $l - th$ equilibrium Equations (6) and (7) from the $m - th$ component of $\mathbf{u}^{(j)}(z)$ (Equation (36)). In particular, the term $f(z)(...)$ stands for pre-multiplication of the function $f(z)$ by the $m - th$ component of $\mathbf{u}^{(j)}(z)$; the term $g(z)(...)_{,z}$ stands for pre-multiplication of the function $g(z)$ by the first derivative of the $m - th$ component of $\mathbf{u}^{(j)}(z)$ with respect to z; the term $g(z)(...)_{,z}$ stands for pre-multiplication of the function $h(z)$ by the second derivative of the $m - th$ component of $\mathbf{u}^{(j)}(z)$ with respect to z.

Appendix B.2. Boundary Conditions

Boundary conditions operators relevant to the present treatment, Equations (6) and (7), are reported in the following:

- Free edge

$$\mathcal{B}^{(j)}_{11} = E_1\mathcal{A}^{(j)}_{11}(...) + E_2\mathcal{A}^{(j)}_{21}(...) \tag{54}$$

$$\mathcal{B}^{(j)}_{12} = E_2\mathcal{A}^{(j)}_{22}(...) \tag{55}$$

$$\mathcal{B}^{(j)}_{13} = E_1\mathcal{A}^{(j)}_{13}(...) + E_2\mathcal{A}^{(j)}_{23}(...) \tag{56}$$

$$\mathcal{B}^{(j)}_{21} = E_3\mathcal{A}^{(j)}_{31}(...) \tag{57}$$

$$\mathcal{B}^{(j)}_{22} = E_3\mathcal{A}^{(j)}_{32}(...) \tag{58}$$

$$\mathcal{B}^{(j)}_{31} = E_7\mathcal{A}^{(j)}_{71}(...) \tag{59}$$

$$\mathcal{B}^{(j)}_{33} = E_7\mathcal{A}^{(j)}_{73}(...) \tag{60}$$

$$\mathcal{B}^{(j)}_{34} = E_7\mathcal{A}^{(j)}_{74}(...) \tag{61}$$

$$\mathcal{B}^{(j)}_{44} = \frac{t^2}{6}\left[E_1\mathcal{A}^{(j)}_{44}(...) + E_2\mathcal{A}^{(j)}_{54}(...)\right] \tag{62}$$

$$\mathcal{B}^{(j)}_{45} = \frac{t^2}{6}E_2\mathcal{A}^{(j)}_{55}(...) \tag{63}$$

$$\mathcal{B}^{(j)}_{54} = \frac{t^2}{6}\left[E_3\mathcal{A}^{(j)}_{44}(...) + E_3\mathcal{A}^{(j)}_{54}(...)\right] \tag{64}$$

$$\mathcal{B}^{(j)}_{55} = \frac{t^2}{6}E_3\mathcal{A}^{(j)}_{55}(...) \tag{65}$$

- Simply supported edge

$$\mathcal{B}^{(j)}_{11} = \mathcal{B}^{(j)}_{22} = \mathcal{B}^{(j)}_{33} = \mathcal{B}^{(j)}_{55} = 1 \tag{66}$$

$$\mathcal{B}^{(j)}_{44} = \frac{t^2}{6}\left[E_1\mathcal{A}^{(j)}_{44}(...) + E_2\mathcal{A}^{(j)}_{54}(...)\right] \tag{67}$$

$$\mathcal{B}^{(j)}_{45} = \frac{t^2}{6}E_2\mathcal{A}^{(j)}_{55}(...) \tag{68}$$

- Sliding edge

$$\mathcal{B}^{(j)}_{11} = \mathcal{B}^{(j)}_{22} = \mathcal{B}^{(j)}_{44} = \mathcal{B}^{(j)}_{55} = 1 \tag{69}$$

$$\mathcal{B}^{(j)}_{31} = E_7\mathcal{A}^{(j)}_{71}(...) \tag{70}$$

$$\mathcal{B}^{(j)}_{33} = E_7\mathcal{A}^{(j)}_{73}(...) \tag{71}$$

$$\mathcal{B}^{(j)}_{34} = E_7\mathcal{A}^{(j)}_{74}(...) \tag{72}$$

- Clamped edge

$$\mathcal{B}^{(j)}_{11} = \mathcal{B}^{(j)}_{22} = \mathcal{B}^{(j)}_{33} = \mathcal{B}^{(j)}_{44} = \mathcal{B}^{(j)}_{55} = 1 \tag{73}$$

References

1. Bellman, R. Differential quadrature and long-term integration. *J. Math. Anal. Appl.* **1971**, *34*, 235–238.
2. Bellman, R.; Kashef, B.G.; Casti, J. Differential quadrature: A technique for the rapid solution of nonlinear partial differential equations. *J. Comput. Phys.* **1972**, *10*, 40–52.
3. Petersen, I. Convergence of approximate methods of the interpolation type for ordinary differential equations. *Izv. Akad. Nauk. SSR* **1961**, *1*, 3–12.
4. Karpilovskaya, E.B. Convergence of the collocation method. *Proc. USSR Acad. Sci.* **1963**, *151*, 766–769.
5. Vainikko, G. Convergence and stability of the collocation method. *Differ. ur-niya* **1965**, *1*, 244–254.
6. Vainikko, G. The convergence of the collocation method for non-linear differential equations. *USSR Comput. Math. Math. Phys.* **1966**, *6*, 47–58.
7. Kaspshitskaya, M.F.; Luchka, A.Y. The collocation method. *USSR Comput. Math. Math. Phys.* **1968**, *8*, 19–39.
8. Schillinger, D.; Evans, J.A.; Reali, A.; Schott, M.; Hughes, T.J.R. Isogeometric collocation: Cost comparison with galerkin methods and extension to adaptive hierarchical nurbs discretizations. *Comput. Methods Appl. Mech. Eng.* **2013**, *267*, 170–232.
9. Bert, C.W.; Malik, M. Differential quadrature: A powerful new technique for analysis of composite structures. *Compos. Struct.* **1997**, *39*, 179– 189.
10. Mirfakhraei, P.; Redekop, D. Buckling of circular cylindrical shells by the differential quadrature method. *Int. J. Press. Vessel. Pip.* **1998**, *75*, 347–353.
11. Wu, T.; Liu, G. Axisymmetric bending solution of shells of revolution by the generalized differential quadrature rule. *Int. J. Press. Vessel. Pip.* **2000**, *77*, 149–157.
12. Wu, T.; Wang, Y.; Liu, G. A generalized differential quadrature rule for bending analysis of cylindrical barrel shells. *Comput. Methods Appl. Mech. Eng.* **2003**, *192*, 1629–1647.
13. Artioli, E.; Viola, E. Static analysis of shear-deformable shells of revolution via G.D.Q. method. *Struct. Eng. Mech.* **2005**, *19*, 459– 475.
14. Viola, E.; Artioli, E. The G.D.Q. method for the harmonic dynamic analysis of rotational shell structural elements. *Struct. Eng. Mech.* **2004**, *17*, 789–817.
15. Artioli, E.; Gould, P. L.; Viola, E. A differential quadrature method solution for shear-deformable shells of revolution. *Eng. Struct.* **2005**, *27*, 1879–1892.
16. Artioli, E.; Viola, E. Free vibration analysis of spherical caps using a G.D.Q. numerical solution. *ASME J. Press. Vessel. Technol.* **2006**, *128*, 370–378.
17. Bellman, R.; Kashef, B.; Lee, E.; Vasudevan, R. Differential quadrature and splines. *Comput. Math. Appl.* **1975**, *1*, 371–376.
18. Guo, Q.; Zhong, H. Non-linear vibration analysis of beams by a spline-based differential quadrature method. *J. Sound Vib.* **2004**, *269*, 413–420.
19. Zhong, H. Spline-based differential quadrature for fourth order differential equations and its application to kirchhoff plates. *Appl. Math. Model.* **2004**, *28*, 353–366.
20. Huang, D. Analysis of laminated plates and shells by using spline gauss collocation method. *Comput. Struct.* **1991**, *38*, 469–473.
21. Viswanathan, K.; Lee, S.K. Free vibration of laminated cross-ply plates including shear deformation by spline method. *Int. J. Mech. Sci.* **2007**, *49*, 352–363.
22. Viswanathan, K.; Navaneethakrishnan, P. Free vibration study of layered cylindrical shells by collocation with splines. *J. Sound Vib.* **2003**, *260*, 807–827.
23. Viswanathan, K.; Navaneethakrishnan, P. Free vibration of layered truncated conical shell frusta of differently varying thickness by the method of collocation with cubic and quintic splines. *Int. J. Solids Struct.* **2005**, *42*, 1129–1150.
24. Bazilevs, Y.; Calo, V.M.; Cottrell, J.A.; Evans, J.A.; Hughes, T.J.R.; Lipton, S.; Scott, M.A.; Sederberg, T.W. Isogeometric analysis using t-splines. *Comput. Methods Appl. Mech. Eng.* **2010**, *199*, 229–263.
25. Cottrell, J.A.; Hughes, T. J.R.; Reali, A. Studies of refinement and continuity in isogeometric structural analysis. *Comput. Methods Appl. Mech. Eng.* **2007**, *196*, 4160–4183.
26. Cottrell, J.A.; Reali, A.; Bazilevs, Y.; Hughes, T. J.R. Isogeometric analysis of structural vibrations. *Comput. Methods Appl. Mech. Eng.* **2006**, *195*, 5257–5296.

27. Hughes, T. J.R.; Cottrell, J.A.; Bazilevs, Y. Isogeometric analysis: Cad, finite elements, nurbs, exact geometry and mesh refinement. *Comput. Methods Appl. Mech. Eng.* **2005**, *194*, 4135–4195.

28. Hughes, T.J.R.; Reali, A.; Sangalli, G. Duality and unified analysis of discrete approximations in structural dynamics and wave propagation: Comparison of p-method finite elements with k-method nurbs. *Comput. Methods Appl. Mech. Eng.* **2008**, *197*, 4104–4124.

29. Hughes, T. J.R.; Reali, A.; Sangalli, G. Efficient quadrature for nurbs-based isogeometric analysis. *Comput. Methods Appl. Mech. Eng.* **2010**, *199*, 301–313.

30. Auricchio, F.; da Veiga, L.B.; Hughes, T. J. R.; Reali, A.; Sangalli, G. Isogeometric collocation methods. *Math. Models Methods Appl. Sci.* **2010**, *20*, 2075–2107.

31. Auricchio, F.; da Veiga, L.B.; Hughes, T. J. R.; Reali, A.; Sangalli, G. Isogeometric collocation for elastostatics and explicit dynamics. *Comput. Methods Appl. Mech. Eng.* **2012**, *249–252*, 2–14.

32. Auricchio, F.; da Veiga, L.B.; Kiendl, J.; Lovadina, C.; Reali, A. Locking-free isogeometric collocation methods for spatial timoshenko rods. *Comput. Methods Appl. Mech. Eng.* **2013**, *263*, 113–126.

33. Da Veiga, L.B.; Lovadina, C.; Reali, A. Avoiding shear locking for the timoshenko beam problem via isogeometric collocation methods. *Comput. Methods Appl. Mech. Eng.* **2012**, *241–244*, 38–51.

34. Da Veiga, L.B.; Lovadina, C. An interpolation theory approach to shell eigenvalue problems. *Math. Models Methods Appl. Sci.* **2008**, *18*, 2003–2018.

35. Finlayson, B.; Scriven, L. The method of weighted residuals—A review. *Appl. Mech. Rev.* **1966**, 19, 735–748.

36. Farin, G. *Curves and Surfaces for Computer Aided Geometric Design;* Morgan Kaufman Publishers: San Francisco, CA, USA, 2002.

37. Gould, P.L. *Finite Element Analysis of Shells of Revolution*; Pitman Advanced Publishing Program: New York, NY, USA, 1985.

38. Kraus, H. *Thin Elastic Shells*; John Wiley & Sons: New York, NY, USA, 1967.

39. Novozhilov, V.V. *Thin Shell Theory*; Wolters-Noordhoff: Groningen, The Netherlands, 1970.

40. Soedel, W. *Vibrations of Shells and Plates*; Marcel Dekker, Inc.: New York, NY, USA, 2004.

41. Piegl, L.; Tiller, W. *The NURBS Book*, 2nd ed.; Springer-Verlag: Berlin Heidelberg Germany, 1997.

42. Rogers, D. *An Introduction to NURBS with Historical Perspective*; Morgan Kaufman Publishers: San Francisco, CA, USA, 2001.

43. Greville, T. On the normalization of the b-splines and the location of the nodes for the case of unequally spaced knots. In *Inequalities*; Oshida, O., Ed.; Academic Press: New York, NY, USA, 1967.

44. Bellomo, N. Nonlinear models and problems in applied sciences from differential quadrature to generalized collocation methods. *Math. Comput. Model.* **1997**, *26*, 13–34.

45. Bellomo, N.; De Angelis, E.; Graziano, L.; Romano, A. Solution of nonlinear problems in applied sciences by generalized collocation methods and mathematica. *Comput. Math. Appl.* **2001**, *41*, 1343–1363.

46. Johnson, R.W. Higher order b-spline collocation at the greville abscissae. *Appl. Numer. Math.* **2005**, *52*, 63–75.

47. Artioli, E.; da Veiga, L.B.; Hakula, H.; Lovadina, C. Free vibrations for some koiter shells of revolution. *Appl. Math. Lett.* **2008**, *21*, 1245–1248.

48. Auricchio, F.; da Veiga, L.B.; Lovadina, C. Remarks on the asymptotic behaviour of Koiter shells. *Comput. Struct.* **2002**, *80*, 735–745.

49. Da Veiga, L.B.; Lovadina, C. Asymptotics of shell eigenvalue problems. *C. R. Math.* **2006**, *342*, 707–710.

50. Artioli, E.; da Veiga, L.B.; Hakula, H.; Lovadina, C. On the asymptotic behaviour of shells of revolution in free vibration. *Comput. Mech.* **2009**, *44*, 45–60.

51. Altman, W.; Neto, E.L. Vibration of thin shells of revolution based on a mixed finite element formulation. *Comput. Struct.* **1986**, *23*, 291–303.

52. Kunieda, H. Flexural axisymmetric free vibrations of a spherical dome: exact results and approximate solutions. *J. Sound Vib.* **1984**, *92*, 1–10.

53. Luah, M.H.; Fan, S.C. General free vibration analysis of shells of revolution using the spline finite element method. *Comput. Struct.* **1989**, *33*, 1153–1162.

54. Kim, J.G.; Kim, Y.Y. Higher-order hybrid-mixed axisymmetric thick shell element for vibration analysis. *Int. J. Numer. Meth. Eng.* **2001**, *51*, 241–252.

55. Timoshenko, S.; Woinowsky-Krieger, S. *Theory of Plates and Shells*; Mcgraw-Hill: New York, NY, USA, 1959.

56. Reddy, J.N. *Energy and Variational Methods in Applied Mechanics*; John Wiley & Sons: New York, NY, USA, 1984.

57. Kim, J.G.; Kim, Y.Y. A higher-order hybrid-mixed harmonic shell-of-revolution element. *Comp. Meth. Appl. Mech. Eng.* **2000**, *182*, 1–16.

58. Luah, M.H.; Fan, S.C. New spline finite element for analysis of shells of revolution. *J. Eng. Mech. ASCE* **1990**, *116*, 709–725.

59. Basu, P.K.; Gould, P.L. *Shore-III: Shell of Revolution Finite Element Program*; Washington University: St. Louis, MO, USA, 1977.

60. Gould, P. L. *Analysis of Shells and Plates*; Springer-Verlag: New York, NY, USA, 1988.